



Research Article

# Plant synthesis of silver nanoparticles for the pathogen inhibition of Gram-positive and Gram-negative bacteria

Leda Georgia Bousiakou<sup>a,b,\*</sup>

<sup>a</sup>Physics Department, College of Science and General Studies, Alfaisal University, P.O. Box 50927, Riyadh 11533, Saudi Arabia

<sup>b</sup>IMD Laboratories, Lefkippos Technology Park, National Centre for Scientific Research-NCSR Demokritos, Agia Paraskevi, GR-15130 Athens, Greece

## ARTICLE INFO

### Keywords:

Antibacterial activity  
Escherichia coli  
GO nanosheets  
Pseudomonas aeruginosa  
Silver nanoparticle  
Staphylococcus aureus

## ABSTRACT

It is well known that both silver nanoparticles (AgNPs) possess broad spectrum antibacterial properties, having a multimodal action that leads to cell death. This work focuses on the preparation and characterization of AgNPs via the green synthesis route, assessing their effectiveness towards the inhibition of Gram-positive and Gram-negative bacteria, namely *Escherichia Coli*, *Staphylococcus Aureus*, and *Pseudomonas Aeruginosa*. In particular, after preparation, the AgNPs are characterized using scanning electron microscopy (SEM-EDS), X-ray diffraction (XRD) as well as dynamic light scattering (DLS), showing that the majority of nanoparticles are in the 20nm range with spherical or pseudo-spherical shapes. Clinical isolates of *Escherichia coli*, *Staphylococcus aureus*, and *Pseudomonas aeruginosa* were subsequently exposed to varying concentrations of AgNPs (0.25–1.5 mg/ml) and incubated at 37 °C for 24 h to assess their antimicrobial activity. The results showed that the highest antibacterial activity was against the bacterium *Staphylococcus aureus*, while *Pseudomonas aeruginosa* was the least affected. AgNPs with an average diameter of approximately 20 nm are regarded as optimal for antibacterial applications, being overall less toxic to mammalian cells and the environment compared to AgNP sizes of <10 nm. Furthermore, a comparison of zones of inhibition (ZOI) resulting from the use of AgNPs is compared to those of graphene oxide (GO) nanosheets with varying oxygen content from literature, showing that while using the same protocols, AgNPs outperform GO across all tested strains and concentrations.

## 1. Introduction

Silver (Ag) is a well-known antibacterial agent that has been used historically as silver nitrate or silver sulfadiazine to combat bacterial infections in different cream preparations (Rai *et al.*, 2009), (Morones *et al.*, 2005), (Clement & Jarrett, 1994). With the emergence of nanotechnology, Ag nanoparticles (NPs) attracted significant attention for their antibacterial and antifungal activity towards several drug-resistant pathogens that pose a universal threat according to the World Health Organization (WHO). It has been estimated that by 2050, the death toll attributed to antimicrobial resistance will reach 10 million worldwide, with costs estimated at €1.5 billion annually due to the increase in healthcare costs (WHO, 2021). As a result, the demand for developing new antimicrobial therapies has become crucial. In particular, the enhanced efficacy of silver nanoparticles (AgNPs), relative to bulk silver, is primarily attributed to their increased surface-area-to-volume ratio. This structural characteristic promotes a more sustained and controlled release of Ag<sup>+</sup> ions, which are the primary active agents in antimicrobial activity. In contrast, bulk silver tends to release a rapid initial burst of Ag<sup>+</sup> ions, which may induce immediate antibacterial effects but lack long-term efficacy.

Investigations into the antibacterial mechanisms of AgNPs reveal a multimodal mode of action, including disruption of bacterial cell morphology and membrane integrity (Fig. 1), along with inhibition of ATP synthesis and interference with DNA replication (Pal *et al.*, 2007;

Yin *et al.*, 2020). Moreover, it has been hypothesized that AgNPs with antibacterial properties could potentially eliminate the evolution of resistant bacteria, since they target multiple biomolecules at once, avoiding the development of resistant strains.

In particular, when studying the antimicrobial mechanism of AgNPs, it is important to consider that the specific bacterial response can vary based on the bacterial type, i.e., Gram-positive and Gram-negative (More *et al.*, 2023), (Humagain, 2018).

In general, Gram-positive bacteria are characterized by a thick, semipermeable peptidoglycan layer in their cell walls, which increases their susceptibility to interaction with AgNPs. *Staphylococcus aureus* has, in particular, a peptidoglycan layer ~ 80 nm in thickness, containing covalently bound teichoic and teichuronic acids, significantly thicker than that of Gram-negative bacteria (Humagain, 2018). This layer contains phosphate and carboxyl groups that, at physiological pH, can lead to a strong negative charge on their surface, allowing the binding via electrostatic forces to Ag<sup>(+)</sup> ions. On the other hand, Gram-negative bacteria are covered with an outer membrane of lipopolysaccharides (Silhavy *et al.*, 2010), which is inherently non-permeable, providing them with an extra layer of defence.

Nevertheless, despite the protective role of the bacterial outer membrane, its inherent negative charge enables electrostatic interactions with positively charged silver ions (Ag<sup>+</sup>) released from AgNPs. These interactions can disrupt membrane integrity, leading to the generation of reactive oxygen species (ROS) and subsequent

### \*Corresponding author:

E-mail address: leda07@hotmail.com (L Bousiakou)

Received: 06 August, 2025 Accepted: 26 October, 2025 Epub Ahead of Print: 19 February, 2026 Published: 24 February, 2026

DOI: 10.25259/JKSUS\_1274\_2025

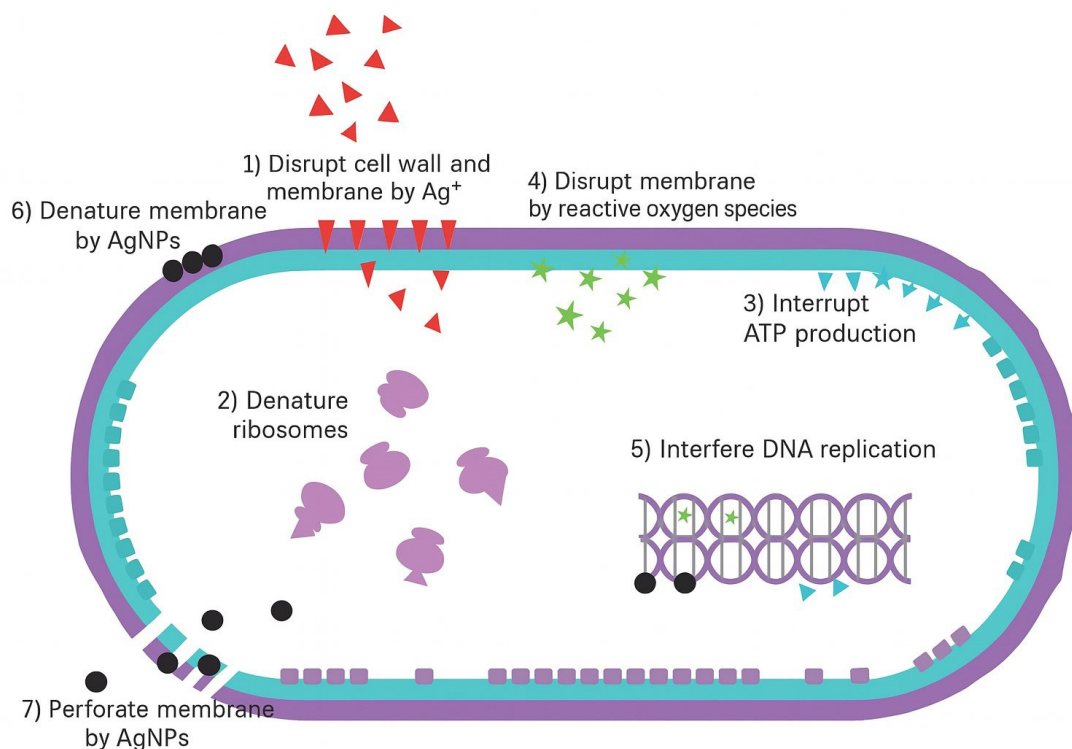


Fig. 1. The multimodal antibacterial mechanism of AgNPs adapted from (Yin *et al.*, 2020).

cellular damage. A widely recognized antimicrobial mechanism of AgNPs involves the adhesion of  $\text{Ag}^+$  ions to the bacterial membrane, facilitating their insertion into the lipid bilayer. This results in membrane depolarization, increased permeability, and structural compromise, ultimately interfering with essential metabolic functions and culminating in cell death (Sánchez-López *et al.*, 2020; Huq *et al.*, 2020; Mendes *et al.*, 2022).

Evidence also indicates that various ROS, generated at the nanoparticle surface, contribute to membrane damage of both Gram-positive and negative bacteria by increasing permeability. Specifically, AgNPs, owing to their high surface energy, can act as electron donors or acceptors. This redox activity facilitates catalytic interactions with molecular oxygen and water, leading to the formation of superoxide anions ( $\text{O}_2^-$ ), hydrogen peroxide ( $\text{H}_2\text{O}_2$ ), and hydroxyl radicals ( $\cdot\text{OH}$ ), all of which play a key role in oxidative stress-mediated bacterial inactivation (Kim *et al.*, 2009).

Moreover, the direct permeability of bacterial cells to AgNPs is a critical factor in their antimicrobial efficacy. Studies indicate that in Gram-positive bacteria, the thick yet porous peptidoglycan layer permits only nanoparticles smaller than 20 nm to access the cytoplasmic membrane directly (Slavin *et al.*, 2017). In the case of Gram-negative bacteria, the presence of narrow porin channels further restricts permeability, typically requiring ultrasmall nanoparticles in the 1–3 nm range to traverse the outer membrane and exert intracellular effects.

However, AgNPs in the 1–3 nm range exhibit markedly higher toxicity toward bacterial cells, but also pose increased risks to mammalian cells and the environment when compared to larger nanoparticles in the 20 nm range and above (Kim *et al.*, 2012). Their high surface reactivity leads to excessive silver ion ( $\text{Ag}^+$ ) release, oxidative stress, and unintended toxicity to non-target organisms. In contrast, AgNPs in the 20 nm range offer a well-controlled rate of ion release, sufficient to inhibit bacterial growth while minimizing damage to host cells and reducing ecological risks. Furthermore, they are less likely to directly penetrate eukaryotic cells and can aggregate more readily, which limits their bioavailability in the environment. These characteristics make them safer and a more practical alternative for applications where a balance between efficacy and biocompatibility is essential.

Currently, there are various ways to synthesize AgNP, using both chemical or physical routes (Lekha *et al.*, 2021). The physical routes

lead to high-purity AgNPs and include ball milling, laser ablation, and sputtering. Nevertheless, they come at a high cost and involve complex procedures at high temperature and pressure (Tien *et al.*, 2008; Stagon & Huang, 2013; Amendola & Meneghetti, 2009). On the other hand, while certain chemical synthesis methods, such as electrochemical, sol-gel, and chemical reduction approaches, may be more cost-effective, they often involve hazardous reagents that generate toxic byproducts, posing significant environmental risks (Duman *et al.*, 2024; Kumari *et al.*, 2023; Mallick *et al.*, 2004). For that purpose, green synthesis has attracted significant attention, using extracts from various plants, microbial cells, and biopolymers (Castillo-Henriquez *et al.*, 2020; Zuhrotun *et al.*, 2023). These can act as reducing agents, aiding the transformation of salt precursors to nanoparticles, allowing for an environmentally friendly production approach. If we consider also that during the last 15 years, the market of AgNPs has been growing steadily, with an estimated production of > 500 tons per year to supply industry demands, we can appreciate the significance of lowering the toxicity of such processes to the environment. In general, when using green synthesis, plant extracts can be mixed with a solution of the metal salt at room temperature (Fig. 2). In particular, plant extracts contain compounds with reducing properties, such as flavonoids, polyphenols, alkaloids, and terpenoids. These can help reduce silver ions ( $\text{Ag}^+$ ) to form AgNPs ( $\text{Ag}^0$ ). Apart from AgNP, a lot of other NP, such as gold, have been produced this way.

Green tea is an excellent choice as it contains a high amount of polyphenols such as catechins that act both as a reducing agent of

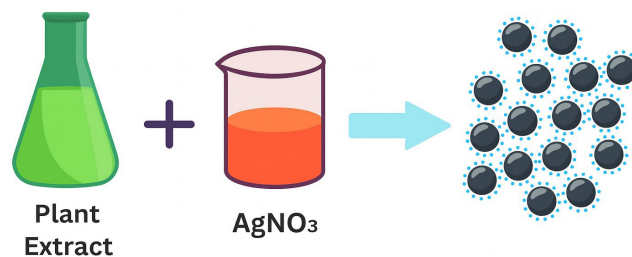


Fig. 2. Green synthesis of nanoparticles. reducing silver ions ( $\text{Ag}^+$ ) to form ( $\text{Ag}^0$ ).

the salt precursors to form AgNP, but also act as stabilizing agents in the synthesis of nanoparticles (Thatyana *et al.*, 2023). In particular, epigallocatechin gallate (EGCG) can reduce silver ions ( $\text{Ag}^+$ ) to form AgNPs as well as stabilize them by forming a protective layer around them, preventing aggregation (Sökmen *et al.*, 2017).

In this work, we prepare AgNP using the green synthesis route and test their antibacterial action in both Gram-positive and Gram-negative bacteria. Subsequently, we compare their efficiency to low and high oxygen content GO nanosheets from literature (Bousiakou *et al.*, 2022) using the same protocols, in order to gauge their usage as wide-spectrum antibacterial agents.

## 2. Materials and Methods

AgNPs are prepared using green tea leaves, and their morphology, elemental profile, structure, and size are investigated. For that purpose, scanning electron microscopy (SEM-EDS), X-ray diffraction (XRD), and dynamic light scattering (DLS) are utilized. All reagents were purchased from Sigma Aldrich- Merck, unless otherwise indicated.

Dried green tea leaves (*Camellia sinensis*) were initially ground into a fine powder using a blender, followed by further refinement with a mortar and pestle to achieve a uniform particle size. Subsequently, 10 g of the resulting powder were decocted in 100 mL of distilled water at 100°C for 20 min. The resulting extract was filtered using standard laboratory filtration techniques, transferred into a conical flask, and stored at 4°C for further use. Finally, 15 mL of the green tea extract was added to a 100 mL volume of 2mM  $\text{AgNO}_3$  solution under magnetic stirring at 30°C. The AgNPs were isolated by centrifugation at 14,000 rpm using an IKA-GL centrifuge, and the resulting pellet was oven-dried for 20 min, yielding a deposit of AgNPs for subsequent characterization.

SEM was performed using a Hitachi Regulus 8100 SEM to explore the morphology of the produced AgNPs, while EDS was also employed for elemental analysis. Furthermore, the structural characteristics of the AgNPs were observed using XRD. In particular, a Bruker D8 Discoverer diffractometer was used applying CuK $\alpha$  radiation ( $\lambda = 1.5418 \text{ \AA}$ ).

Bacterial cultures and Kirby-Bauer disk diffusion tests were conducted following the procedure outlined in Bousiakou *et al.*, 2022 to assess the antimicrobial activity of AgNPs. Specifically, inocula were prepared from clinical strains of *Escherichia coli*, *Staphylococcus aureus*, and *Pseudomonas aeruginosa* by gently collecting bacterial colonies with a sterile loop and suspending them in saline solution. Cell densities were adjusted to 0.5 McFarland standard (approximately  $10^8$  CFU/mL) using a McFarland Biosan 1B Densitometer. From each bacterial suspension, 100  $\mu\text{L}$  was evenly spread onto agar plates using sterile swabs. Separately, AgNPs were sonicated in Millipore water, and 20  $\mu\text{L}$  of each sample was pipetted onto sterile 6 mm Whatman No. 1 filter paper discs. This process was repeated for four different AgNP concentrations: 0.25 mg/mL, 0.5 mg/mL, 1 mg/mL, and 1.5 mg/mL, as described in Bousiakou *et al.*, 2022. The impregnated discs were carefully placed onto the inoculated agar plates using sterilized forceps. The plates were then incubated at 37°C for over 24 h. Following incubation, the diameters of the inhibition zones around each disc were measured using a Vernier caliper. Millipore water served as the negative control, consistently producing no inhibition zones ( $0.00 \pm 0.00$  mm) in all experiments.

## 3. Results

### 3.1 Energy-dispersive X-ray (EDS) analysis

EDS analysis showed a strong peak at 3keV, that confirms the presence of elemental silver as in Fig. 3. In particular, peaks between 2.7keV and 3.5keV are indicative of the formation of AgNPs arising from surface plasmon resonance (SPR) (Sharma *et al.*, 2009). In the EDS spectrum, we note the presence of weaker signals of the following elements: Ca (4.22%), Mg (0.26%), Cl (0.47%), Ca (4.22%), and O (26.47%) that could originate as residual plant biomolecules involved in the reduction process and trace minerals present in biological materials (Fig. 4).

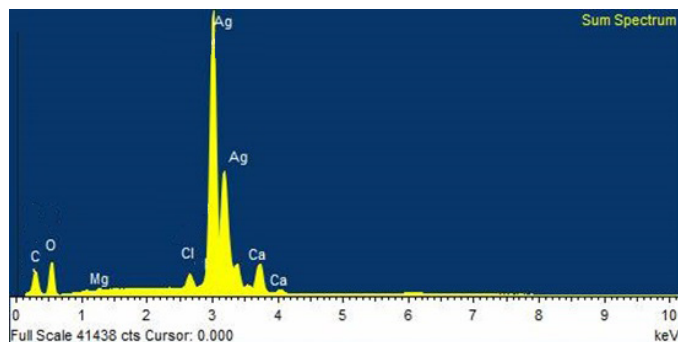


Fig. 3. EDS spectrum confirming the presence of elemental silver (Ag) as the dominant component. Minor peaks for C, O, Cl, Mg, and Ca are observed as residual elements from the green synthesis process. The x-axis represents energy (keV), and the y-axis represents intensity (counts)..

Element	App	Intensity	Weight%	Weight%	Atomic%
	Conc.	Corrn.		Sigma	
C K	65.09	1.2377	4.85	0.10	14.53
O K	99.18	0.3453	26.47	0.24	59.55
Mg K	1.64	0.5813	0.26	0.03	0.39
Cl K	4.76	0.9297	0.47	0.03	0.48
Ca K	38.89	0.8485	4.22	0.04	3.79
Ag L	639.14	0.9243	63.73	0.23	21.27
Totals			100.00		

Fig. 4. EDS elemental composition table of green-synthesized AgNPs. Silver (Ag) is the predominant element by weight (63.73%), with oxygen and carbon indicating plant-derived biomolecules.

### 3.2 Scanning electron microscopy and zeta potential analysis

SEM showed that the AgNPs nanoparticles appear mostly spherical or quasi-spherical, indicating a controlled growth (Fig. 5). The dispersion is relatively uniform with some degree of agglomeration in the brighter clustered regions. An estimation suggests particle sizes range from 20 to ~30 nm, with occasional larger agglomerates. This size range and structure are consistent with green synthesis at moderate precursor levels.

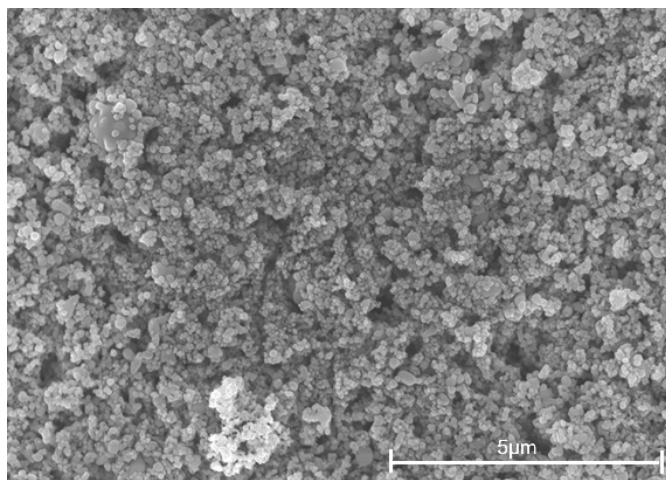


Fig. 5. The image, taken at 10,000 $\times$  magnification with a 5  $\mu\text{m}$  scale bar, shows predominantly spherical AgNPs with moderate agglomerates.

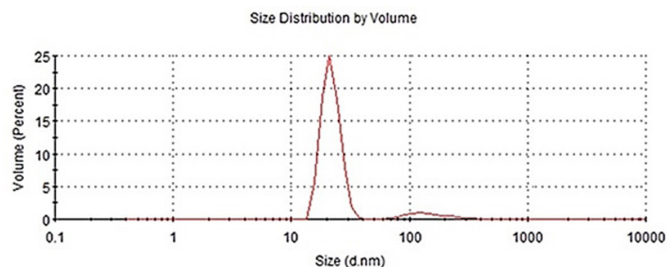


Fig. 6. DLS spectrum showing the particle size distribution in distilled water at 25°C using Zetasizer® software.

### 3.3 Zeta-potential and dynamic light scattering characterization

The particle size distribution was further evaluated by DLS (Zetasizer Nano S, Malvern Instruments, Malvern, UK) at PH=7 in double-distilled water (Fig. 6). The DLS volume-based size distribution graph shows a dominant sharp peak at around 25–30 nm, corresponding to the well-dispersed nanoparticle population. A small peak between 50–150 nm corresponds to agglomeration events. These results align with SEM observations, confirming the dual presence of well-formed nanoparticles and weakly-bound clusters.

### 3.4 X-ray diffraction analysis

The XRD peaks 38.18°, 44.3°, 64.74°, 77.48°, and 81.41° can be attributed to the Ag(111), Ag(200), Ag(220), and Ag(311) crystallographic planes, respectively, indicating that the AgNPs are face-centered cubic and crystalline in nature (Shameli et al., 2012). There were no other phases identified as impurities in the XRD spectrum (Fig. 7).

### 3.5 Antibacterial activity of the AgNP nanoparticles

During incubation, AgNPs diffuse from the impregnated disks into the surrounding agar medium, where they exert antimicrobial activity by inhibiting bacterial proliferation. The diameter of the resulting zone of inhibition serves as a quantitative indicator of the agent's antibacterial potency, with larger zones reflecting higher efficacy. The control used in all cases was Millipore water, which yielded a 0.00±0.00 inhibition zone. Table 1 below summarizes the antibacterial activity of AgNPs against both Gram-positive and Gram-negative bacterial strains.

The results indicate that AgNPs show the highest antibacterial activity against the Gram-positive bacterium *Staphylococcus aureus*, followed by *Escherichia coli* and *Pseudomonas aeruginosa*, which are both Gram-negative. This difference can be attributed to the structural characteristics of Gram-negative bacteria, which possess an outer membrane that limits nanoparticle penetration. Nevertheless, AgNPs remain highly effective across all tested strains due to their mechanisms of ion release, oxidative mechanisms, and protein interaction. In particular, Fig. 8 shows that *Escherichia coli* initially has greater susceptibility than

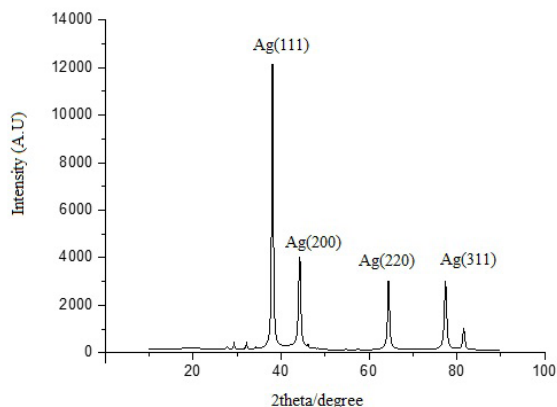


Fig. 7. XRD pattern of synthesized silver (Ag) nanoparticles.

Table 1.

The antibacterial activity of AgNPs against *Escherichia coli*, *Staphylococcus aureus*, and *Pseudomonas aeruginosa*.

Bacteria	Gram type	Concentration (mg/mL)	AgNP ZOI (mm)
<i>S. aureus</i>	Gram-positive	0.25	26.0 ± 0.4
		0.5	29.2 ± 0.5
		1.0	31.5 ± 0.4
		1.5	36.0 ± 0.3
<i>E. coli</i>	Gram-negative	0.25	20.1 ± 0.3
		0.5	22.8 ± 0.4
		1.0	25.3 ± 0.4
		1.5	28.2 ± 0.3
<i>P. aeruginosa</i>	Gram-negative	0.25	14.3 ± 0.2
		0.5	17.0 ± 0.3
		1.0	22.8 ± 0.4
		1.5	26.5 ± 0.3

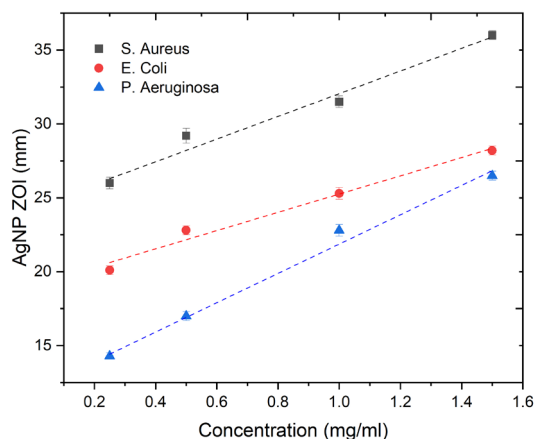


Fig. 8. This figure illustrates the antibacterial activity of AgNPs across three bacterial strains.

*Pseudomonas aeruginosa* at lower AgNP concentrations, possibly due to its relatively more permeable membrane. In this regard, even though porins do not directly transport nanoparticles, they can influence nanoparticle effectiveness by controlling the uptake of released silver ions ( $\text{Ag}^+$ ) (Nikaido et al., 2003). In particular, *P. aeruginosa* has much lower outer membrane permeability than *Escherichia coli*, partly due to its fewer, narrower, and more selective porins (e.g., OprD, OprB, OprO/P) that restrict antibiotic influx (Ferenci & Phan, 2015). One study reports its permeability is only about 8% of that of *Escherichia coli* (Chevalier et al., 2017). Another parameter could be that *Escherichia coli* bacteria have less efficient efflux pumps compared to *Pseudomonas aeruginosa* (Poole, 2001). Again, efflux pumps affect AgNPs indirectly, since AgNPs themselves are, in general, too large to be actively transported by these systems. However, efflux pumps play a critical role in the bacterial response to ( $\text{Ag}^+$ ) ions released from the nanoparticles. In particular, silver ions ( $\text{Ag}^+$ ) released from AgNPs can be exported by certain efflux systems, reducing intracellular toxicity (Silver, 2003; Randall et al., 2015). These efflux systems can export  $\text{Ag}^+$  ions out of the cell, reducing intracellular accumulation. It has been shown that while *E. Coli* exhibits ( $\text{Ag}^+$ ) and ( $\text{Cu}^+$ ) ion resistance, *Pseudomonas aeruginosa* has more advanced, broader-spectrum metal efflux systems making it more resistant to silver ions and other toxic metals (Franke et al., 2003), (Nies, 2003). However, at higher concentrations, AgNPs can more effectively penetrate and disrupt *Pseudomonas aeruginosa* outer defenses, by overwhelming efflux pumps. Thus, as the AgNP concentration increases, the effectiveness of their antibacterial mechanisms intensifies, overcoming *Pseudomonas aeruginosa* defenses more effectively and leading to larger ZOIs.

This response (Fig. 8) highlights the potential of AgNPs to combat even highly resistant Gram-negative pathogens when applied at sufficient concentrations. It also underscores the importance of dose optimization in nanoparticle-based antibacterial treatments. Finally, it should be noted that AgNPs in the 20 nm range provide sufficient silver ion release, increasing contact points with the bacterial envelope and allowing multiple simultaneous mechanisms to act. Even though nanoparticles below 10 nm are, in general, known for stronger antibacterial activity, they pose a higher risk of toxicity to human cells and the environment. Therefore, within the context of antibacterial applications, 20 nm AgNPs offer an optimal balance between efficacy and safety (Lok et al., 2006; Clement & Jarrett, 1994).

### 3.6 A comparison of the antibacterial activity of AgNP and GO nanosheets at 15% and 39% oxygen content.

A comparison of the antibacterial activity of AgNPs and graphene oxide (GO) nanosheets is presented, based on identical protocols for culture preparation and antimicrobial concentration, as described in Bousiakou et al., 2022. In particular, as seen in Table 2, GO with 15% oxygen content consistently shows lower antibacterial activity compared to GO with 39% oxygen content due to its reduced oxygen functional group density. Higher oxygenation enhances GO's ability to produce ROS, improve dispersion in aqueous environments, and increase its interactions with bacterial membranes. Nevertheless, it is evident that AgNPs outperform both GO variants across all tested strains and concentrations.

In particular, the comparison between GO and AgNPs in terms of zone of inhibition ZOI is also rooted in their distinct antibacterial mechanisms and relative efficacy reported across numerous studies (Liu et al., 2011; Yadav et al., 2017). More specifically, the antibacterial action of GO is primarily due to mechanical stress (sharp edges), oxidative stress, and cell membrane wrapping. The level of oxygen functional groups affects the generation of ROS and the membrane disruption ability. Higher oxygen content (as in GO 39%) correlates with improved antibacterial activity, but effectiveness varies depending on the bacterial strain and GO dispersion quality. In the case of AgNPs, it is known that they exhibit a multi-modal antibacterial effect, including the release of Ag<sup>+</sup> ions as well as significant ROS generation, often greater than that of GO. AgNPs can interfere with protein function and cell wall integrity, cause DNA damage, and respiratory inhibition in bacteria (Malik et al., 2022). In multiple comparative studies, AgNPs consistently show larger ZOIs than GO when tested against *Pseudomonas aeruginosa*, *E. coli*, and *Staphylococcus aureus*, particularly at higher concentrations (Prasad et al., 2017). The data in Table 2 shows GO (39%) achieving 12.02 mm at 0.25 mg/ml, increasing to 23.11 mm at 1.5 mg/mL. In contrast, AgNPs at similar concentrations show a ZOI of 14.3–26.5 mm, reflecting

**Table 2.**

Comparison of the zones of inhibition in all three bacterial species in the presence of Ag nanoparticles and GO (15% and 39%).

Bacteria	Gram type	Conc. (mg/mL)	GO 15% ZOI (mm)	GO 39% ZOI (mm)	AgNP ZOI (mm)
<i>S. aureus</i>	Gram-positive	0.25	10.53 ± 0.24	22.88 ± 0.19	26.0 ± 0.4
		0.5	12.74 ± 0.31	25.10 ± 0.26	29.2 ± 0.5
		1.0	13.15 ± 0.12	26.90 ± 0.14	31.5 ± 0.4
		1.5	15.27 ± 0.18	31.42 ± 0.17	36.0 ± 0.3
<i>E. coli</i>	Gram-negative	0.25	8.03 ± 0.17	17.10 ± 0.14	20.1 ± 0.3
		0.5	9.44 ± 0.21	19.22 ± 0.16	22.8 ± 0.3
		1.0	10.92 ± 0.11	20.37 ± 0.19	25.3 ± 0.4
		1.5	12.77 ± 0.15	24.11 ± 0.23	28.2 ± 0.3
<i>P. aeruginosa</i>	Gram-negative	0.25	7.43 ± 0.17	12.02 ± 0.13	14.3 ± 0.2
		0.5	8.54 ± 0.10	14.11 ± 0.23	17.0 ± 0.3
		1.0	11.02 ± 0.16	21.20 ± 0.19	22.8 ± 0.4
		1.5	12.27 ± 0.21	23.11 ± 0.17	26.5 ± 0.3

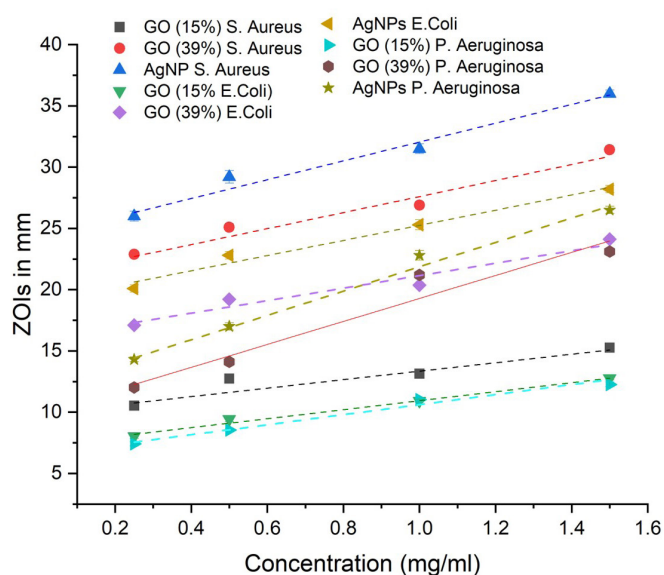


**Fig. 9.** This figure shows the antibacterial activity of GO (15% and 39%) and AgNPs against three bacterial strains.

stronger and broader-spectrum activity, particularly against Gram-negative bacteria like *P. aeruginosa*. These mechanisms enable AgNPs to overcome structural barriers in Gram-negative bacteria, such as the outer membrane found in *Escherichia coli* and *Pseudomonas aeruginosa*, which typically reduces susceptibility to other antimicrobials. In Gram-positive bacteria like *Staphylococcus aureus*, which lack an outer membrane, all three materials perform better, though AgNPs still show the strongest effect (Fig. 9). The superior efficacy of AgNPs, especially in higher concentrations, demonstrates their potential as a broad-spectrum antibacterial.

## 4. Conclusions

In this work, AgNPs were successfully synthesized using green tea extract, which acted both as a reducing and stabilizing agent. Characterization through SEM-EDS, DLS, and XRD confirmed that the nanoparticles were mostly spherical with an average size in the 20 nm range. The antibacterial assays demonstrated that AgNPs exert significant inhibition effects on both Gram-positive and Gram-negative bacteria. The highest ZOI was observed against *Staphylococcus aureus*, a Gram-positive bacterium, while *Pseudomonas aeruginosa*, known for its robust outer membrane, exhibited the least susceptibility, particularly at lower AgNP concentrations. Moreover, the results showed a dose-dependent increase in antibacterial efficacy across all tested strains. When compared to GO nanosheets of varying oxygen content, AgNPs consistently outperformed both 15% and 39% of GO in terms of ZOI values. While higher oxygenated GO showed improved bacterial inhibition compared to lower oxygenated GO due to increased ROS generation, AgNPs remained superior across all tested conditions. These findings confirm that AgNPs synthesized via green routes represent a viable and environmentally friendly alternative to conventional antibiotics, especially for multidrug-resistant pathogens. Furthermore, their superior performance compared to GO nanosheets underscores their potential as next-generation broad-spectrum antimicrobial agents. Future research could explore under the same conditions the synergistic formulations combining AgNPs and GO to harness the strength of both nanomaterials.

## CRedit authorship contribution statement

**Leda Georgia Bousiakou:** Conceptualization, Methodology, Investigation, Formal analysis, Data curation, Writing – original draft, Writing – review and editing, Visualization, Funding acquisition.

## Declaration of competing interests

The author declares that there are no known competing financial interests or personal relationships that could have appeared to influence the work reported in this paper.

## Data availability

The data supporting the findings of this study are available from the author upon reasonable request.

## Declaration of generative AI and AI-assisted technologies in the writing process

The authors confirm that there was no use of artificial intelligence (AI)-assisted technology for assisting in the writing or editing of the manuscript and no images were manipulated using AI.

## Acknowledgement

The author gratefully acknowledges Alfaisal University, Riyadh, Kingdom of Saudi Arabia, for supporting the publication fees of this article.

## References

- Amendola, V., Meneghetti, M., 2009. Laser ablation synthesis in solution and size manipulation of noble metal nanoparticles. *Phys Chem Chem Phys* 11, 3805-3821. <https://doi.org/10.1039/b900654k>
- Bousiakou, L.G., Qindeel, R., Al-Dossary, O.M., Kalkani, H., 2022. Synthesis and characterization of graphene oxide (GO) sheets for pathogen inhibition: *Escherichia coli*, *Staphylococcus aureus* and *Pseudomonas aeruginosa*. *J King Saud Univ Sci* 34, 102002. <https://doi.org/10.1016/j.jksus.2022.102002>
- Castillo-Henriquez, L., Alfaro-Aguilar, K., Ugalde-Álvarez, J., Vega-Fernández, L., Montes de Oca-Vásquez, G., Vega-Baudrit, J.R., 2020. Green synthesis of gold and silver nanoparticles from plant extracts and their possible applications as antimicrobial agents in the agricultural area. *Nanomaterials (Basel)* 10, 1763. <https://doi.org/10.3390/nano10091763>
- Chevalier, S., Bouffartigues, E., Bodilis, J., Maillot, O., Lesouhaitier, O., Feuilloley, M.G.J., Orange, N., Dufour, A., Cornelis, P., 2017. Structure, function and regulation of *Pseudomonas aeruginosa* porins. *FEMS Microbiol Rev* 41, 698-722. <https://doi.org/10.1093/femsre/fux020>
- Clement, J.L., Jarrett, P.S., 1994. Antibacterial silver. *Met Based Drugs* 1, 467-482. <https://doi.org/10.1155/MBD.1994.467>
- Duman, H., Eker, F., Akdaşci, E., Witkowska, A.M., Bechelany, M., Karav, S., 2024. Silver nanoparticles: A comprehensive review of synthesis methods and chemical and physical properties. *Nanomaterials (Basel)* 14, 1527. <https://doi.org/10.3390/nano14181527>
- Ferenci, T., Phan, K., 2015. How porin heterogeneity and trade-offs affect the antibiotic susceptibility of gram-negative bacteria. *Genes (Basel)* 6, 1113-1124. <https://doi.org/10.3390/genes6041113>
- Franke, S., Grass, G., Rensing, C., Nies, D.H., 2003. Molecular analysis of the copper-transporting efflux system CusCFBA of *Escherichia coli*. *J Bacteriol* 185, 3804-3812. <https://doi.org/10.1128/JB.185.13.3804-3812.2003>
- Humagain, S., 2018. Differences between Gram-positive and Gram-negative bacteria. Online Science Notes. Available from: <https://onlinesciencenotes.com/differences-between-gram-positive-and-gram-negative-bacteria/> (accessed 01 July 2025).
- Huq, M.A., 2020. Green synthesis of silver nanoparticles using *Pseudoduganella eburnea* MAHUQ-39 and their antimicrobial mechanisms investigation against drug resistant human pathogens. *Int J Mol Sci* 21, 1510. <https://doi.org/10.3390/ijms21041510>
- Kim, S., Choi, J.E., Choi, J., Chung, K.H., Park, K., Yi, J., Ryu, D.Y., 2009. Oxidative stress-dependent toxicity of silver nanoparticles in human hepatoma cells. *Toxicol In Vitro* 23, 1076-1084. <https://doi.org/10.1016/j.tiv.2009.06.001>
- Kim, T.H., Kim, M., Park, H.S., Shin, U.S., Gong, M.S., Kim, H.W., 2012. Size-dependent cellular toxicity of silver nanoparticles. *J Biomed Mater Res A* 100, 1033-1043. <https://doi.org/10.1002/jbm.a.34053>
- Kumari, S., Raturi, S., Kulshrestha, S., Chauhan, K., Dhingra, S., Andrés, K., Thu, K., Khargotra, R., Singh, T., 2023. A comprehensive review on various techniques used for synthesizing nanoparticles. *J Mater Res Technol* 27, 1739-1763. <https://doi.org/10.1016/j.jmrt.2023.09.291>
- Lekha, D.C., Shanmugam, R., Madhuri, K., Dwarampudi, L.P., Bhaskaran, M., Kongara, D., Tesfaye, J.L., Nagaprasad, N., Bhargavi, V.L.N., Krishnaraj, R., 2021. Review on silver nanoparticle synthesis method, antibacterial activity, drug delivery vehicles, and toxicity pathways: Recent advances and future aspects. *J Nanomater* 2021, 1-11. <https://doi.org/10.1155/2021/4401829>
- Liu, S., Zeng, T.H., Hofmann, M., Burcombe, E., Wei, J., Jiang, R., Kong, J., Chen, Y., 2011. Antibacterial activity of graphite, graphite oxide, graphene oxide, and reduced graphene oxide: Membrane and oxidative stress. *ACS Nano* 5, 6971-6980. <https://doi.org/10.1021/nn202451x>

- Lok, C.N., Ho, C.M., Chen, R., He, Q.Y., Yu, W.Y., Sun, H., Tam, P.K., Chiu, J.F., Che, C.M., 2006. Proteomic analysis of the mode of antibacterial action of silver nanoparticles. *J Proteome Res* 5, 916-924. <https://doi.org/10.1021/pr0504079>
- Mallick, K., Witcomb, M.J., Scurrall, M.S., 2004. Polymer stabilized silver nanoparticles: A photochemical synthesis route. *J Mater Sci* 39, 4459-4463. <https://doi.org/10.1023/b:jmsc.0000034138.80116.50>
- Malik, S.B., Saggi, J.I., Gul, A., Abbasi, B.A., Iqbal, J., Waris, S., Jordan, Y.A.B., Chalhah, W., 2022. Synthesis and characterization of silver and graphene nanocomposites and their antimicrobial and photocatalytic potentials. *Molecules* 27, 5184. <https://doi.org/10.3390/molecules27165184>
- Mendes, C., Thirupathi, A., Corrêa, M.E.A.B., Gu, Y., Silveira, P.C.L., 2022. The use of metallic nanoparticles in wound healing: new perspectives. *Int J Mol Sci* 23, 15376. <https://doi.org/10.3390/ijms232315376>
- Morones, J.R., Elechiguerra, J.L., Camacho, A., Holt, K., Kouri, J.B., Ramirez, J.T., Yacaman, M.J., 2005. The bactericidal effect of silver nanoparticles. *Nanotechnology* 16, 2346-2353. <https://doi.org/10.1088/0957-4484/16/10/059>
- More, P.R., Pandit, S., Filippis, A., Franci, G., Mijakovic, I., Galdiero, M., 2023. Silver nanoparticles: Bactericidal and mechanistic approach against drug resistant pathogens. *Microorganisms* 11, 369. <https://doi.org/10.3390/microorganisms11020369>
- Nies, D.H., 2003. Efflux-mediated heavy metal resistance in prokaryotes. *FEMS Microbiol Rev* 27, 313-339. [https://doi.org/10.1016/S0168-6445\(03\)00048-2](https://doi.org/10.1016/S0168-6445(03)00048-2)
- Nikaido, H., 2003. Molecular basis of bacterial outer membrane permeability revisited. *Microbiol Mol Biol Rev* 67, 593-656. <https://doi.org/10.1128/MMBR.67.4.593-656.2003>
- Pal, S., Tak, Y.K., Song, J.M., 2007. Does the antibacterial activity of silver nanoparticles depend on the shape of the nanoparticle? A study of the Gram-negative bacterium *Escherichia coli*. *Appl Environ Microbiol* 73, 1712-1720. <https://doi.org/10.1128/AEM.02218-06>
- Poole, K., 2001. Multidrug resistance in Gram-negative bacteria. *Curr Opin Microbiol* 4, 500-508. [https://doi.org/10.1016/S1369-5274\(00\)00242-3](https://doi.org/10.1016/S1369-5274(00)00242-3)
- Prasad, K., Lekshmi, G.S., Ostrikov, K., Lussini, V., Blinco, J., Mohandas, M., Vasilev, K., Bottle, S., Bazaka, K., Ostrikov, K., 2017. Synergic bactericidal effects of reduced graphene oxide and silver nanoparticles against Gram-positive and Gram-negative bacteria. *Sci Rep* 7, 1591. <https://doi.org/10.1038/s41598-017-01669-5>
- Rai, M., Yadav, A., Gade, A., 2009. Silver nanoparticles as a new generation of antimicrobials. *Biotechnol Adv* 27, 76-83. <https://doi.org/10.1016/j.biotechadv.2008.09.002>
- Randall, C.P., Gupta, A., Jackson, N., Busse, D., O'Neill, A.J., 2015. Silver resistance in Gram-negative bacteria: A dissection of endogenous and exogenous mechanisms. *J Antimicrob Chemother* 70, 1037-1046. <https://doi.org/10.1093/jac/dku523>
- Sánchez-López, E., Gomes, D., Esteruelas, G., Bonilla, L., Lopez-Machado, A.L., Galindo, R., Cano, A., Espina, M., Etcheto, M., Camins, A., Silva, A.M., Durazzo, A., Santini, A., Garcia, M.L., Souto, E.B., 2020. Metal-based nanoparticles as antimicrobial agents: An overview. *Nanomaterials (Basel)* 10, 292. <https://doi.org/10.3390/nano10020292>
- Shameli, K., Ahmad, M.B., Zamanian, A., Sangpour, P., Shabanzadeh, P., Abdollahi, Y., Zargar, M., 2012. Green biosynthesis of silver nanoparticles using curcuma longa tuber powder. *Int J Nanomedicine* 7, 5603-5610. <https://doi.org/10.2147/IJN.S36786>
- Sharma, V.K., Yngard, R.A., Lin, Y., 2009. Silver nanoparticles: Green synthesis and their antimicrobial activities. *Adv Colloid Interface Sci* 145, 83-96. <https://doi.org/10.1016/j.cis.2008.09.002>
- Silhavy, T.J., Kahne, D., Walker, S., 2010. The bacterial cell envelope. *Cold Spring Harb Perspect Biol* 2, a000414. <https://doi.org/10.1101/cshperspect.a000414>
- Silver, S., 2003. Bacterial silver resistance: Molecular biology and uses and misuses of silver compounds. *FEMS Microbiol Rev* 27, 341-353. [https://doi.org/10.1016/S0168-6445\(03\)00047-0](https://doi.org/10.1016/S0168-6445(03)00047-0)
- Slavin, Y.N., Asnis, J., Häfeli, U.O., Bach, H., 2017. Metal nanoparticles: Understanding the mechanisms behind antibacterial activity. *J Nanobiotechnology* 15, 65. <https://doi.org/10.1186/s12951-017-0308-z>
- Sökmen, M., Alomar, S.Y., Albay, C., Serdar, G., 2017. Microwave assisted production of silver nanoparticles using green tea extracts. *J Alloys Compd* 725, 190-198. <https://doi.org/10.1016/j.jallcom.2017.07.094>
- Stagon, S.P., Huang, H., 2013. Syntheses and applications of small metallic nanorods from solution and physical vapor deposition. *Nanotechnol Rev* 2, 259-267. <https://doi.org/10.1515/ntrev-2013-0001>
- Thatyana, M., Dube, N.P., Kemboi, D., Manicum, A.E., Mokgalaka-Fleischmann, N.S., Tembu, J.V., 2023. Advances in phytonanotechnology: A plant-mediated green synthesis of metal nanoparticles using *Phyllanthus* plant extracts and their antimicrobial and anticancer applications. *Nanomaterials (Basel)* 13, 2616. <https://doi.org/10.3390/nano13192616>
- Tien, D.C., Liao, C.Y., Huang, J.C., Tseng, K.H., Lung, J.K., Tsung, T.T., Kao, W.S., Tsai, T.H., Cheng, T.W., Yu, B.S., Lin, H.M., Stobinski, L., 2008. Novel technique for preparing a nano-silver water suspension by the arc-discharge method. *Rev Adv Mater Sci* 18, 752-758.
- World Health Organization (WHO). Global antimicrobial resistance and use surveillance system (GLASS) report. 2021. World Health Organization, Geneva.
- Yadav, N., Dubey, A., Shukla, S., Saini, C.P., Gupta, G., Priyadarshini, R., Lochab, B., 2017. Graphene oxide-coated surface: inhibition of bacterial biofilm formation due to specific surface-interface interactions. *ACS Omega* 2, 3070-3082. <https://doi.org/10.1021/acsomega.7b00371>
- Yin, I.X., Zhang, J., Zhao, I.S., Mei, M.L., Li, Q., Chu, C.H., 2020. The antibacterial mechanism of silver nanoparticles and its application in dentistry. *Int J Nanomedicine* 15, 2555-2562. <https://doi.org/10.2147/IJN.S246764>
- Zuhrotun, A., Oktaviani, D.J., Hasanah, A.N., 2023. Biosynthesis of gold and silver nanoparticles using phytochemical compounds. *Molecules* 28, 3240. <https://doi.org/10.3390/molecules28073240>